JPE 19-5-6

https://doi.org/10.6113/JPE.2019.19.5.1122
ISSN(Print): 1598-2092 / ISSN(Online): 2093-4718

Analysis and Design of Transformer Windings Schemes in Multiple-Output Flyback Auxiliary Power Supplies with High-Input Voltage

Xianzeng Meng*, Chunyan Li*, Tao Meng†, and Yanhua An*

†,*School of Mechanical and Electrical Engineering, Heilongjiang University, Harbin, China

Abstract

In this paper, aiming at high-voltage applications, transformer windings schemes of multiple-output two-transistor flyback converters are investigated, which are mainly based on the stray capacitances effect. First, based on a transformer model including equivalent stray capacitors, the operational principle of the converter is presented, and the main influence of its stay capacitors is determined. Second, the windings structures of the transformer are analyzed and designed based on the stray capacitances effect. Third, the windings arrangements of the transformer are analyzed and designed through a coupling analysis of the secondary windings and a stray capacitance analysis between the primary and secondary windings. Finally, the analysis and design conclusions are verified by experimental results obtained from a 60W laboratory prototype of a multiple-output two-transistor flyback converter.

Key words: Multiple-output auxiliary power supply, Stray capacitance, Transformer, Two-transistor flyback, Winding arrangement

I. INTRODUCTION

Nowadays, the applications of high dc input voltage are gradually increasing. With the rapid development in the power electronics field, more and more high-voltage converters have been adopted. Presently, the main research focus for high voltage converters is reducing the voltage stress of power devices. Among the existing solutions, the series-switches, multiple-level and input-series schemes have been widely investigated. For the series-switches scheme, special passive or active balancing methods must be introduced to achieve the voltage balance of each switch. This results in additional losses and restricts the switching frequency. For the traditional multiple-level scheme, as the "level" increases, the flying capacitors or clamping diodes increase, and the control strategy becomes more complex. For the conventional input-series scheme, an input voltage sharing controller must be introduced to ensure the voltage balance, which makes the control circuits relatively complex [1]-[5].

Presently, investigations of high-voltage converters are mainly aiming at medium-power or high-power applications. There are fewer studies on low-power applications.

An auxiliary power supply is a typical application of low-power converters, where the flyback topology is usually adopted. Typical investigations of auxiliary power supplies in high-voltage applications are as follows. In [1], a flyback converter with series switches was presented. In [6] and [7], wide-range input voltage single-transistor and two-transistor flyback auxiliary power supplies were designed for high-voltage power electronics equipment, respectively. In [8], a flyback auxiliary power supply was presented for photovoltaic systems. An input-series flyback converter with a decoupled master/slave control strategy was proposed in [9]. Input-series flyback auxiliary power supplies were presented for solid state transformers in [10] and [11]. A high voltage input-series power supply was proposed for the gate driving of SiC devices in [12]. Input-series multiple-output flyback auxiliary power supplies were proposed in [13] and [14].

Presently, investigations of high-voltage auxiliary power supplies mainly focus on the voltage stress of each power device. However, very few studies focus on their high-frequency

Manuscript received Jan. 4, 2019; accepted May 29, 2019
Recommended for publication by Associate Editor Hongfei Wu.
†Corresponding Author: mengtao@hit.edu.cn
Tel: +86-451-86609437, Fax: +86-451-86609437, Heilongjiang University
*School of Mechanical and Electrical Engineering, Heilongjiang University, China

© 2019 KIPE

transformer.

For flyback auxiliary power supplies, the design of the transformer is very important. With increases in the switching frequency, the operation of converters is more and more restricted by the parasitic parameters of its transformer. Generally, for high-frequency transformers, there are two main parasitic parameters: the leakage inductance and the stray capacitance [15]-[17]. Traditionally, investigations mainly focus on the leakage inductor in the design process, since the voltage spikes caused by the series resonance between the leakage inductor and the parasitic capacitor of the power switch are very important when it comes to determining the conversion efficiency of a converter [18], [19].

However, the operation of a converter can also be affected by the stray capacitances of its transformer. The basic stray capacitances effect of a flyback transformer can be concluded as follows. 1) In the operational process, some energy is stored in the stray capacitors. Therefore, a large current spike appears in the transformer and power devices when this part of the energy flows instantaneously. As a result, the reliability of the converter decreases. 2) High-frequency resonances appear in the transformer and main circuit when the voltage of each winding is suddenly changed, which results in increased power losses [20]-[25]. Generally, when voltage increases or conversion power decreases, the stray capacitances effect becomes more serious. Therefore, in the high-voltage low-power applications, stray capacitance cannot be ignored in the design process.

In this paper, aiming at high-voltage applications, the transformer windings schemes of multiple-output flyback auxiliary power supplies are analyzed and designed through analysis and comparison of the stray capacitances effect. When compared to the traditional single-transistor flyback topology, due to a much lower voltage stress, the two-transistor flyback topology is better suited for high-input voltage applications. Therefore, this investigation is based on the two-transistor flyback topology.

This paper is organized as follows. In section II, a model of the flyback transformer including equivalent stray capacitors is presented. In section III, windings structures are analyzed based on the stray capacitance effect. The windings arrangements are analyzed and designed in section IV. The analysis and design are verified by experimental results in section V. Finally, some conclusions are given in section VI.

II. Stray Capacitances of the Flyback Transformer

A multiple-output two-transistor flyback converter is shown in Fig. 1, where V_i, V_{o1} and V_{o2} are the input and output voltages (two output circuits are analyzed here); L_p, L_{s1} and L_{s2} are the inductances in the primary and secondary sides of the transformer T; N_p, N_{s1} and N_{s2} (generally, it is designed that: $N_{s1}/N_{s2}=V_{o1}/V_{o2}$) are the turns number of the primary and secondary windings; and L_{lk} is the leakage inductance.

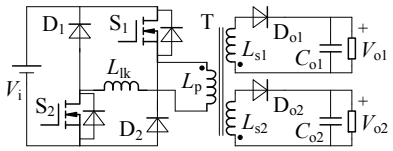

Fig. 1. Two-output two-transistor flyback converter.

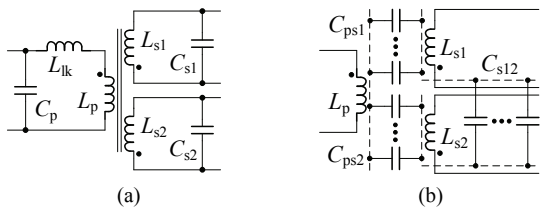

Fig. 2. Stray capacitances of the flyback transformer T. (a) Model with a lumped capacitor in each winding. (b) Stray capacitances distributed between the windings.

For the flyback transformer T, there are stray capacitances within each winding. Generally, these stray capacitances can be simplified as a lumped capacitor in each winding, as shown in Fig. 2(a), where C_p is the stray capacitor of the primary winding, and C_{s1} and C_{s2} are stray capacitors of the secondary windings. Moreover, there are also stray capacitances distributed between any two windings, as shown in Fig. 2(b), where C_{ps1} and C_{ps2} stand for stray capacitances between the primary and secondary windings, and C_{s12} stands for stray capacitance between the secondary windings.

III. Windings Structures

A. Influence of Stray Capacitance in Each Winding

For further analysis, the operational principle of this converter is presented as follows, where the stray capacitors in each winding (C_p, C_{s1} and C_{s2}) are considered. To simplify the analysis, it is assumed that: 1) all of the devices (except for the transformer) are ideal, and 2) the capacitors C_{o1} and C_{o2} are large enough, so the output voltage can be considered a constant value. The following is the operational process of the converter during one switching period, where discontinuous current mode (DCM) operation is considered, and an equivalent circuit of each stage is shown in Fig. 3.

Stage 1 (t_0~t_1): At t_0, S_1 and S_2 are turned on, C_p, C_{s1} and C_{s2} are charged, and their voltage increases immediately from zero. Due to the charging of these capacitors, a large current spike appears in each switch at t_0. Furthermore, in this stage, a high frequency resonance appears between the parasitic inductance of the conduction circuit and these capacitors. Because of the internal resistance, the resonance ends before t_1. At t_1, the voltages of C_p and C_{s1}, and C_{s2} increases to V_i and $-V_iN_{s1}/N_p$, and $-V_iN_{s2}/N_p$, respectively. In this stage, L_p is also charged, and its current increases from zero.

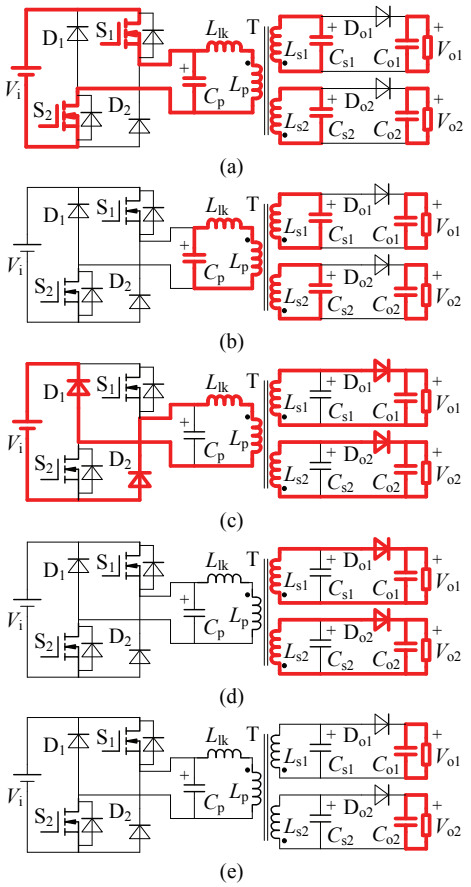

Fig. 3. Equivalent circuit of each stage. (a) Stage 1. (b) Stage 2 and stage 5. (c) Stage 3. (d) Stage 4. (e) Stage 6.

Stage 2 (t_1~t_2): At t_1, S_1 and S_2 are turned off. C_p and C_{s1}, and C_{s2} are resonant with the primary and secondary windings of T, respectively. At t_2, the voltage of C_p and C_{s1}, and C_{s2} are changed into $-V_i$ and V_{o1}, and V_{o2}, respectively.

Stage 3 (t_2~t_3): In this stage, the voltage of C_p and C_{s1}, and C_{s2} are fixed at $-V_i$ and V_{o1}, and V_{o2}, respectively. The energy of L_p is transferred to L_{s1} and L_{s2}. In addition, D_{o1} and D_{o2} are turned on, and the energy is transferred to the load from L_{s1} and L_{s2}. Furthermore, D_1 and D_2 are turned on, and the energy of L_{lk} is transferred back to the input source. At t_3, the current of L_{lk} is reduced to zero.

Stage 4 (t_3~t_4): After t_3, the energy transfer of L_{s1} and L_{s2} is continuous, and current of L_{s1} and L_{s2} is reduced to zero at t_4.

Stage 5 (t_4~t_5): In this stage, C_p and C_{s1}, and C_{s2} are resonant with the primary and secondary windings, respectively. The equivalent circuit of this stage is identical to that of stage 2.

Stage 6 (t_5~t_6): In this stage, the current in primary and secondary sides of T is zero, and voltage of C_p, C_{s1} and C_{s2} are also zero. After t_6, the converter operates in the next period.

It can be seen from the above analysis that the charging and discharging of the stray capacitors (C_p, C_{s1} and C_{s2}) occur in each switching period, and that the operation of the converter is affected by their energy changing. The main influence of this energy are: 1) a large current spike in each switch at the beginning of the turning on state, which is caused by the charging of the stray capacitors in stage 1; and 2) high frequency resonances in the transformer and main circuit, which increase the power losses. For the high frequency transformer, the above influence is more serious when the energy of the stray capacitors increases. Therefore, the energy stored in the stray capacitors should be analyzed and suppressed.

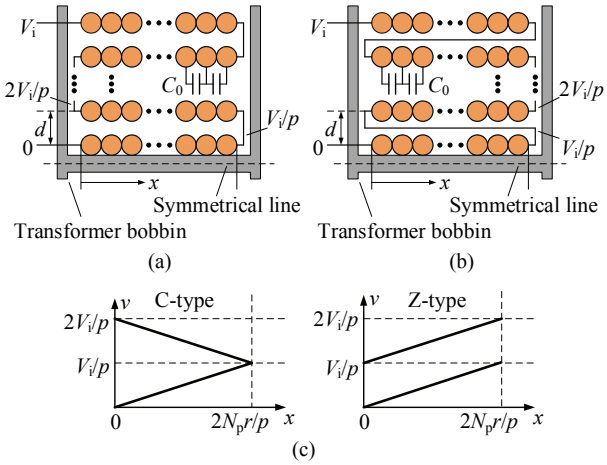

Fig. 4. Two typical multiple-layer winding structures. (a) C-type winding. (b) Z-type winding. (c) Voltage distributions within two adjacent layers.

B. Analysis of Typical Winding Structures

Multiple-layer windings are usually adopted in the transformer of each converter, and are discussed as follows. As shown in Fig. 4 (where the circles represent a cross section of a conductor), there are two typical multiple-layer winding structures: C-type and Z-type structures, where the layer number is p. For these two structures, the voltage and turns number of the winding are V_i and N_p (taking the primary winding as an example). Thus, the voltage and turns number of each layer are V_i/p and N_p/p. Comparatively, the C-type winding is easier to manufacture than the Z-type winding.

For multiple-layer winding, the stray capacitance has two parts: the turn-to-turn and layer-to-layer capacitances. As shown in Fig. 4, it is defined that the stray capacitance of the two adjacent turns in each layer is C_0. Here, it is considered that the winding is rounded tightly. Therefore, C_0 is almost a constant value. For the two winding structures, the energy stored in the turn-to-turn stray capacitance can be calculated:

$$W_{\text{p-tt}} = \frac{1}{2}C_0\left(\frac{V_i}{N_p-1}\right)^2\left(\frac{N_p}{p}-1\right)p = \frac{C_0(N_p-p)V_i^2}{2(N_p-1)^2} \quad (1)$$

For multiple-layer windings, the energy stored in their two adjacent layers can be calculated as follows:

$$W_{\text{p-ll-1}} = \frac{1}{2}\varepsilon\int E^2 \mathrm{d}V \quad (2)$$

where ε is the dielectric constant of the insulation material within the layers, and E is the electric field strength within the layers.

For C-type and Z-type windings, the voltage distribution of two adjacent layers can be expressed as follows:

$$V_{\mathrm{pc}}(x)=\frac{2V_{\mathrm{i}}}{p}-\frac{V_{\mathrm{i}}}{N_{\mathrm{p}}r}x \tag{3}$$

$$V_{\mathrm{pz}}(x)=\frac{V_{\mathrm{i}}}{p} \tag{4}$$

where r is the radius of the conductor.

From (2), (3) and (4), the energy stored in the layer-to-layer stray capacitance of the C-type and Z-type windings can be calculated as follows:

$$W_{\text{pc-ll}}=(p-1)W_{\text{pc-ll-1}}=\frac{(p-1)\varepsilon l}{2d}\int_0^{\frac{2N_{\mathrm{p}}r}{p}}[V_{\mathrm{pc}}(x)]^2\mathrm{d}x=\frac{4(p-1)N_{\mathrm{p}}}{3p^3}\lambda \tag{5}$$

$$W_{\text{pz-ll}}=(p-1)W_{\text{pz-ll-1}}=\frac{(p-1)\varepsilon l}{2d}\int_0^{\frac{2N_{\mathrm{p}}r}{p}}[V_{\mathrm{pz}}(x)]^2\mathrm{d}x=\frac{(p-1)N_{\mathrm{p}}}{p^3}\lambda \tag{6}$$

$$\lambda=\frac{\varepsilon l V_{\mathrm{i}}^2 r}{d} \tag{7}$$

where l is the average length of the coil, and d is the layer-to-layer distance of the winding.

For these two windings, the energy stored in their stray capacitors can be calculated as shown in (8). Generally, the voltage between two adjacent turns is much smaller than that between two adjacent layers. Therefore, $W_{\text{p-tt}}$ is much smaller than $W_{\text{pc-ll}}$ (or $W_{\text{pz-ll}}$), and the energy stored in the stray capacitor is mainly determined by $W_{\text{pc-ll}}$ (or $W_{\text{pz-ll}}$).

$$\begin{cases}W_{\mathrm{pc}}=W_{\text{p-tt}}+W_{\text{pc-ll}}\approx W_{\text{pc-ll}}\\ W_{\mathrm{pz}}=W_{\text{p-tt}}+W_{\text{pz-ll}}\approx W_{\text{pz-ll}}\end{cases} \tag{8}$$

From (5), (6) and (7), it can be seen that the energy stored in the stray capacitor of each winding increases as V_{i} increases. Thus, the influence of this energy is more serious when V_{i} increases. Moreover, it can also be seen that the energy stored in the stray capacitor of each winding has no relationship with the conversion power (P_{o}). When P_{o} decreases, current in the converter decreases accordingly. As a result, the current spike of each switch and the high frequency resonances in the converter caused by this energy become more obvious. Therefore, it can be concluded that the stray capacitances effect is more serious in high-voltage low-power converters. Thus, this energy must be considered during the transformer designing process.

From (5) and (6), a number of things can be seen (it is considered that $p<<N_{\mathrm{p}}$). 1) When p=1, $W_{\text{pc-ll}}=W_{\text{pz-ll}}=0$, and the winding has the minimum energy stored in its stray capacitor. 2) If the turns number (N_{p}) is constant, the energy stored in the stray capacitor decreases when the layer number p increases, as shown in Table I. 3) If the turns number of each layer (N_{p}/p) is constant, the energy stored in the stray capacitor decrease as p increases, as shown in Table II. 4) The energy stored in the stray capacitor of the Z-type winding is slightly lower than that in the stray capacitor of the C-type winding.

TABLE I
VALUES OF $W_{\text{PC-LL}}$ AND $W_{\text{PZ-LL}}$ WHEN N_{P} IS CONSTANT

p	2	3	4	5	6
$W_{\text{pc-ll}}$	$\frac{1}{6}N_{\mathrm{p}}\lambda$	$\frac{8}{81}N_{\mathrm{p}}\lambda$	$\frac{1}{16}N_{\mathrm{p}}\lambda$	$\frac{16}{375}N_{\mathrm{p}}\lambda$	$\frac{5}{162}N_{\mathrm{p}}\lambda$
$W_{\text{pz-ll}}$	$\frac{1}{8}N_{\mathrm{p}}\lambda$	$\frac{2}{27}N_{\mathrm{p}}\lambda$	$\frac{3}{64}N_{\mathrm{p}}\lambda$	$\frac{4}{125}N_{\mathrm{p}}\lambda$	$\frac{5}{216}N_{\mathrm{p}}\lambda$

TABLE II
VALUES OF $W_{\text{PC-LL}}$ AND $W_{\text{PZ-LL}}$ WHEN N_{P}/P IS CONSTANT

p	2	3	4	5	6
$W_{\text{pc-ll}}$	$\frac{1}{3}\frac{N_{\mathrm{p}}}{p}\lambda$	$\frac{8}{27}\frac{N_{\mathrm{p}}}{p}\lambda$	$\frac{1}{4}\frac{N_{\mathrm{p}}}{p}\lambda$	$\frac{16}{75}\frac{N_{\mathrm{p}}}{p}\lambda$	$\frac{5}{27}\frac{N_{\mathrm{p}}}{p}\lambda$
$W_{\text{pz-ll}}$	$\frac{1}{4}\frac{N_{\mathrm{p}}}{p}\lambda$	$\frac{2}{9}\frac{N_{\mathrm{p}}}{p}\lambda$	$\frac{3}{16}\frac{N_{\mathrm{p}}}{p}\lambda$	$\frac{4}{25}\frac{N_{\mathrm{p}}}{p}\lambda$	$\frac{5}{36}\frac{N_{\mathrm{p}}}{p}\lambda$

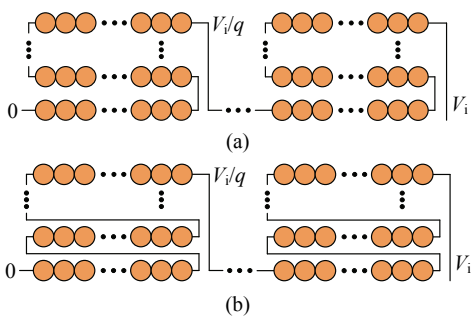

Fig. 5. Segmentation-winding structures. (a) C-type. (b) Z-type.

For the multiple-layer windings, the segmentation structure can also be adopted [19], [21], [26]. The C-type and Z-type segmentation-winding structures are shown in Fig. 5, where the segmentation number is q. The voltage and turns number in each segmentation are V_{i}/q and N_{p}/q. In addition, the voltage and turns number of each layer within one segmentation are V_{i}/pq and N_{p}/pq. According to (1), the energy stored in the turn-to-turn stray capacitance can be calculated:

$$W_{\text{p-ttq}}=\frac{1}{2}C_0\left(\frac{V_{\mathrm{i}}}{N_{\mathrm{p}}-1}\right)^2\left(\frac{N_{\mathrm{p}}}{pq}-1\right)pq=\frac{C_0(N_{\mathrm{p}}-pq)V_{\mathrm{i}}^2}{2(N_{\mathrm{p}}-1)^2} \tag{9}$$

For the segmentation winding, the energy stored in the layer-to-layer stray capacitance is the sum of that in each segmentation. Therefore, according to (5) and (6), the energy stored in the layer-to-layer stray capacitances of the C-type and Z-type segmentation-windings can be obtained as follows:

$$W_{\text{pc-llq}}=\frac{4(p-1)N_{\mathrm{p}}}{3p^3q}\lambda=\frac{4(p-1)\varepsilon l V_{\mathrm{i}}^2 N_{\mathrm{p}}r}{3p^3qd} \tag{10}$$

$$W_{\text{pc-llq}}=\frac{(p-1)N_{\mathrm{p}}}{p^3q}\lambda=\frac{(p-1)\varepsilon l V_{\mathrm{i}}^2 N_{\mathrm{p}}r}{p^3qd} \tag{11}$$

For the segmentation-winding, the energy stored in the stray capacitor is mainly determined by $W_{\text{pc-llq}}$ (or $W_{\text{pz-llq}}$). It can be concluded from (5), (6), (10) and (11) that the energy stored in the stray capacitor of each winding decreases obviously when q increases. However, the winding structure becomes

more complex as q increases.

In the flyback transformer of an auxiliary power supply with a high-input voltage, the voltage and turns number of its primary winding is much larger than those of its secondary windings. Therefore, a number of things can be obtained from the above analysis. 1) For its primary winding, the multiple-layer structure is adopted, and the energy stored in the stray capacitor needs to be suppressed according to the above schemes. 2) For its secondary windings, the single-layer structure can be selected, and the energy stored in the stray capacitors can be ignored.

IV. Windings Arrangements

A. Stray Capacitances Between the Windings

For the stray capacitances distributed between the windings (C_{ps1}, C_{ps2} and C_{s12}) shown in Fig. 2(b), because of electrical isolation, these stray capacitances cannot be analyzed through the storing energy method. However, there are other methods for calculating these capacitances. For example, in [27], evaluation is implemented through an equivalent electrical circuit of the stray capacitances based on the Miller theorem. In this section, the windings arrangements of the transformer are the main focus. Therefore, for the further analysis, only the simplest method for evaluating their capacitances is presented as follows.

Generally, there are two shapes of windings: the rectangular and the round shapes. For example, if an EI-type or EE-type magnetic core is selected for the transformer, rectangular windings are adopted, and if a ETD-type magnetic core is selected, round windings are adopted. For these windings, the parallel-plate and cylindrical models can be used for estimated the stray capacitances between windings, as shown in Fig. 6.

For the rectangular windings, the equivalent stray capacitance between the windings can be estimated as follows (taking the stray capacitance between the primary and secondary windings as an example):

$$C_{ps\text{-}1} = \frac{\varepsilon l_1 h_1}{d_1} \tag{12}$$

where d_1 is the distance between two adjacent layers of the windings, l_1 is the effective length of two adjacent layers, and h_1 is the height of the windings.

For round windings, the equivalent stray capacitance can be estimated as follows:

$$C_{ps\text{-}2} = \frac{2\pi\varepsilon h_1}{\ln(r_2/r_1)} = \frac{2\pi\varepsilon h_1}{\ln[1+(d_1/r_1)]} \tag{13}$$

where r_1 and r_2 (r_2=r_1+d_1) are the radius of the inner and outer layers for the adjacent layers of the windings.

From (12) and (13), it can be seen that the stray capacitance distributed between the windings are mainly determined by the surface area and distance of adjacent layers. It can also be seen that as the area decreases or the distance increases, the stray capacitance decreases.

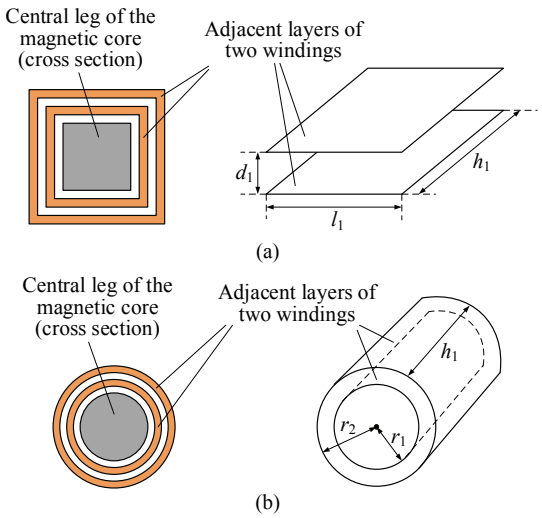

Fig. 6. Two shapes of the windings and their capacitor models. (a) Rectangular windings and a parallel-plate capacitor model. (b) Round windings and a cylindrical capacitor model.

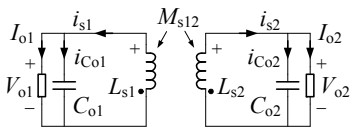

Fig. 7. Simplified circuit in transformer secondary sides.

B. Arrangement of the Secondary Windings

In the transformer of a multiple-output auxiliary power supply, the voltage of its secondary windings is relatively lower. Therefore, the influence of stray capacitances (C_{s1}, C_{s2} and C_{s12}) can be ignored. However, the problem of cross regulation among the output circuits cannot be avoided.

In Fig. 1, the relationship between the two output circuits (N_{s1}/N_{s2}=V_{o1}/V_{o2}) is not always maintained when their conversion powers are independently changed. That is to say, if one output is tightly regulated by feedback control, the other one cannot be a constant output.

During each switching period, two secondary windings of the transformer operate as a coupled-inductor when the switches are turning off. Then a simplified circuit in the transformer secondary sides is shown in Fig. 7, where L_{s1}, L_{s2} and M_{s12} are the self-inductances and the mutual inductance of the two secondary windings. It can be obtained from the basic mathematical model of the coupled-inductor that:

$$\begin{cases} -V_{o1}(t) = L_{s1}\dfrac{\mathrm{d}i_{s1}(t)}{\mathrm{d}t} + M_{s12}\dfrac{\mathrm{d}i_{s2}(t)}{\mathrm{d}t} \\ -V_{o2}(t) = L_{s2}\dfrac{\mathrm{d}i_{s2}(t)}{\mathrm{d}t} + M_{s12}\dfrac{\mathrm{d}i_{s1}(t)}{\mathrm{d}t} \end{cases} \tag{14}$$

$$M_{s12} = k\sqrt{L_{s1}L_{s2}} \tag{15}$$

where k ($0 \le k \le 1$) is the coupling coefficient.

For this flyback transformer, it can be obtained that:

$$\frac{L_{s1}}{L_{s2}}=\frac{N_{s1}^2}{N_{s2}^2} \tag{16}$$

From (14), (15) and (16), the following relationships can be obtained:

$$V_{o2}(t)=\frac{1}{k}\frac{N_{s2}}{N_{s1}}V_{o1}(t)+(\frac{1}{k}-k)\sqrt{L_{s1}L_{s2}}\frac{\mathrm{d}i_{s1}(t)}{\mathrm{d}t} \tag{17}$$

$$V_{o2}(t)=k\frac{N_{s2}}{N_{s1}}V_{o1}(t)-(1-k^2)L_{s2}\frac{\mathrm{d}i_{s2}(t)}{\mathrm{d}t} \tag{18}$$

It is considered that the output voltage V_{o1} is tightly regulated by feedback control. As a result, V_{o1} is constant. When the output current I_{o1} (or I_{o2}) is suddenly changed, the current i_{s1} (or i_{s2}) is changed accordingly during the following switching period. A couple of thinks can be seen from (17) and (18). 1) V_{o2} is affected by the changing of i_{s1} (or i_{s2}). Thus, the relationship $N_{s1}/N_{s2}=V_{o1}/V_{o2}$ cannot be absolutely achieved. 2) The changing of V_{o2} according to the changing of i_{s1} (or i_{s2}) decreases when the coupling coefficient k increases. If k=1 is achieved under ideal conditions, the relationship $N_{s1}/N_{s2}=V_{o1}/V_{o2}$ can be always achieved in the dynamic states.

Therefore, it can be concluded that the secondary windings should be rounded with the smallest distance to increase the coupling coefficient. In this way, a good cross regulation feature can be achieved for the multiple-output circuits.

C. Arrangement of the Primary and Secondary Windings

For the stray capacitances distributed between the primary and secondary windings (C_{ps1} and C_{ps2}), the common mode (CM) electromagnetic interference (EMI) noise is transferred from the input side to the output side of the converter through these capacitors, as shown in Fig. 8(a). This becomes more serious when a high "dv/dt" occurs in the primary side. If the windings structures cannot be arbitrarily changed to suppress these capacitances according to (12) or (13), an additional shielding layer can be added between the windings, as shown in Fig. 8(b). With this, the main EMI noise transferred to the output side can be efficiently eliminated [27]-[30].

According to the above analysis, it can be seen that there are two basic winding-arrangement schemes of this flyback transformer (structure 1: the traditional arrangement; and structure 2: the interleaved arrangement), as shown in Fig.9, where W_p, W_{p1} and W_{p2} stand for the primary windings, and W_s stands for the secondary winding.

In Fig. 9, to increase the coupling coefficient, the secondary windings should be rounded with the smallest equivalent distance. For example, the secondary windings can be connected in paralleled if their turns are similar. For structure 1, the primary winding is rounded in the inner layers, the secondary windings are rounded in the outer layer, and a shielding layer (L_{sh}) is added between them. For structure 2, the primary winding is divided into two parts that are rounded in the inner and outer layers, the secondary windings are rounded in the

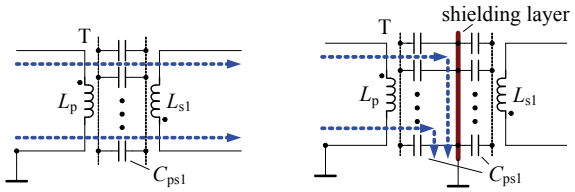

Fig. 8. CM noise transferring through the transformer. (a) Without a shielding layer. (b) With a shielding layer.

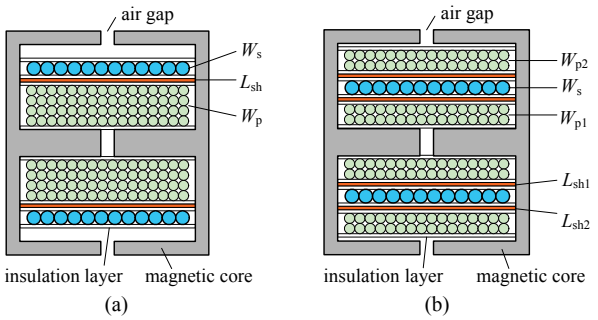

Fig. 9. Two winding-arrangement schemes. (a) Structure 1. (b) Structure 2.

middle layer, and two shielding layers (L_{sh} and L_{sh2}) are added between them. Moreover, due to the high voltage of the primary winding, insulation layers must be introduced. When compared to structure 1, structure 2 has the following features. 1) The surface area between the primary and secondary windings is larger. Therefore, the leakage inductance is smaller. However, the stray capacitance between them is larger. 2) The equivalent two-segmentation structure is adopted in the primary winding. Therefore, the stray capacitance in the primary winding is smaller. However, more shielding and insulation layers must be added. Thus, the winding structure is more complex, and the utilization of the window area of the magnetic core is much lower.

In this flyback converter, the energy of the leakage inductor can be transferred back to the input source. Thus, it is not necessary to reduce the leakage inductance. To reduce the stray capacitance between the primary and secondary windings, simplify the winding structure and increase the utilization of the winding area of the magnetic core. Winding structure 1 is adopted for the transformer here.

V. Experimental Results

To verify the analysis and design, a laboratory-made prototype of a two-transistor flyback auxiliary power supply was built. The main parameters and utilized components of this prototype are: 1) V_i: 300-750Vdc; 2) $V_{o1}=V_{o2}$=24V, I_{o1}=1.5A, I_{o2}=1A and P_{omax}=60W; 3) S_1 and S_2: K1271, the switching frequency is 100kHz; 4) L_p=1.24mH, $L_{s1}=L_{s2}\approx$ 12.5μH; 5) $C_{o1}=C_{o2}$=1000μF.

In this prototype, a traditional peak current controller is

TABLE III
SPECIFIC CHARACTERISTICS OF THE TRANSFORMERS

T	Magnetic core	Primary winding	Two secondary windings	N_p	p
T_a	EE35	C-type	Parallel	120	2
T_b	EE35	C-type	Parallel	240	4
T_c	EI33	C-type	Parallel	120	4
T_d	EI33	Z-type	Parallel	120	4

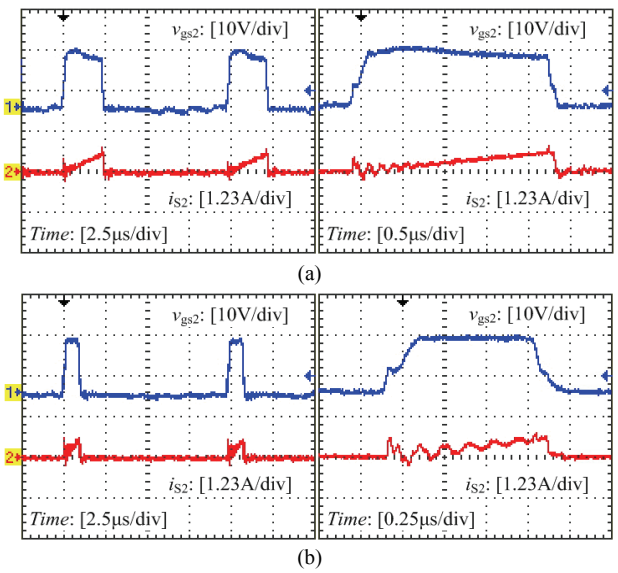

(a) (b)

Fig. 10. Driving and current of S_2 when T_a is adopted (P_o=16W). (a) V_i=300V. (b) V_i=750V.

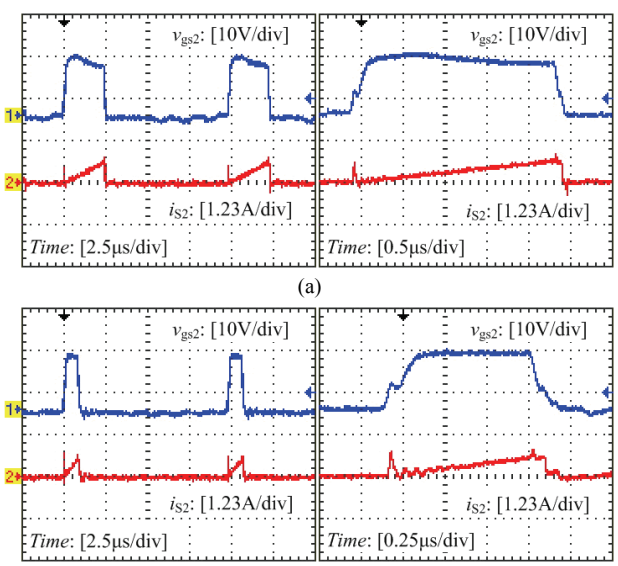

(a) (b)

Fig. 11. Driving and current of S_2 when T_b is adopted (P_o=16W). (a) V_i=300V. (b) V_i=750V.

adopted, and the output voltage V_{o1} is tightly regulated by the feedback control. Furthermore, for a experimental comparison, four flyback transformers (T_a, T_b, T_c and T_d) were made for this prototype. The basic winding arrangements of these

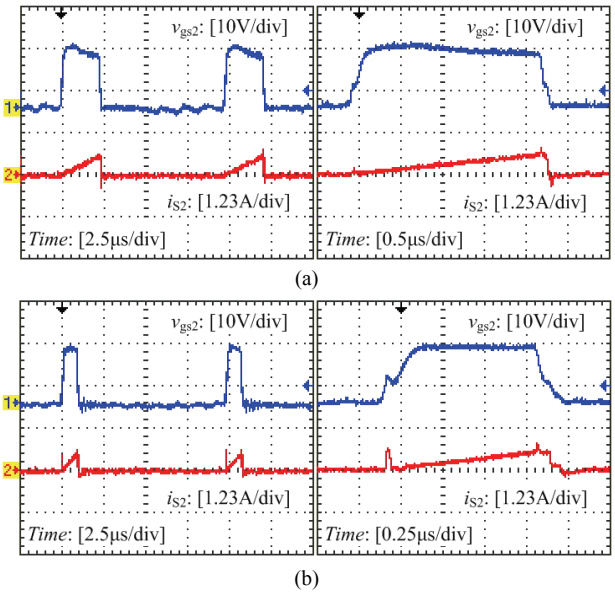

(a) (b)

Fig. 12. Driving and current of S_2 when T_c is adopted (P_o=16W). (a) V_i=300V. (b) V_i=750V.

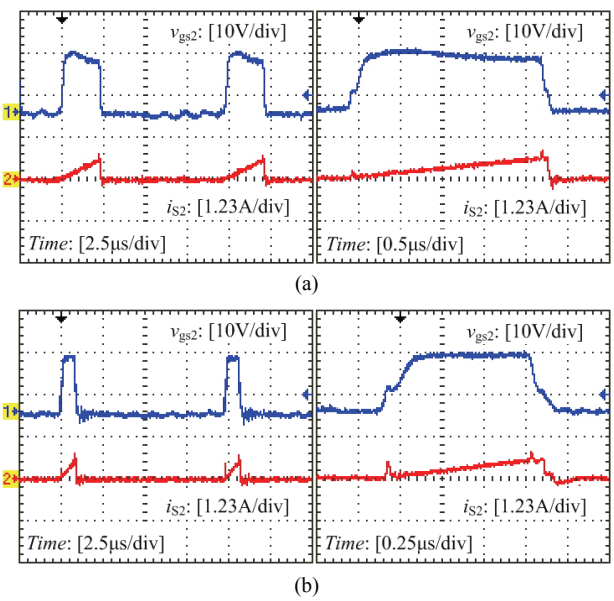

(a) (b)

Fig. 13. Driving and current of S_2 when T_d is adopted (P_o=16W). (a) V_i=300V. (b) V_i=750V.

transformers are shown in Fig. 9(a), and their specific characteristics are shown in Table III.

Figs. 10-13 show driving and current waveforms of S_2 when various transformers are adopted, where the prototype is operated under the light load condition (P_o=16W), and the input voltages (V_i) are 300V and 750V, respectively. From these experimental results, a number of conclusions can be verified. 1) When V_i increases, the stray capacitances effect becomes more serious. 2) From Fig. 10 and 11, it can be seen that if the turns number of each layer (N_p/p) is identical, the influence of the stray capacitors decrease when the layer number p increases. 3) From Figs. 10 and 12, it can be seen

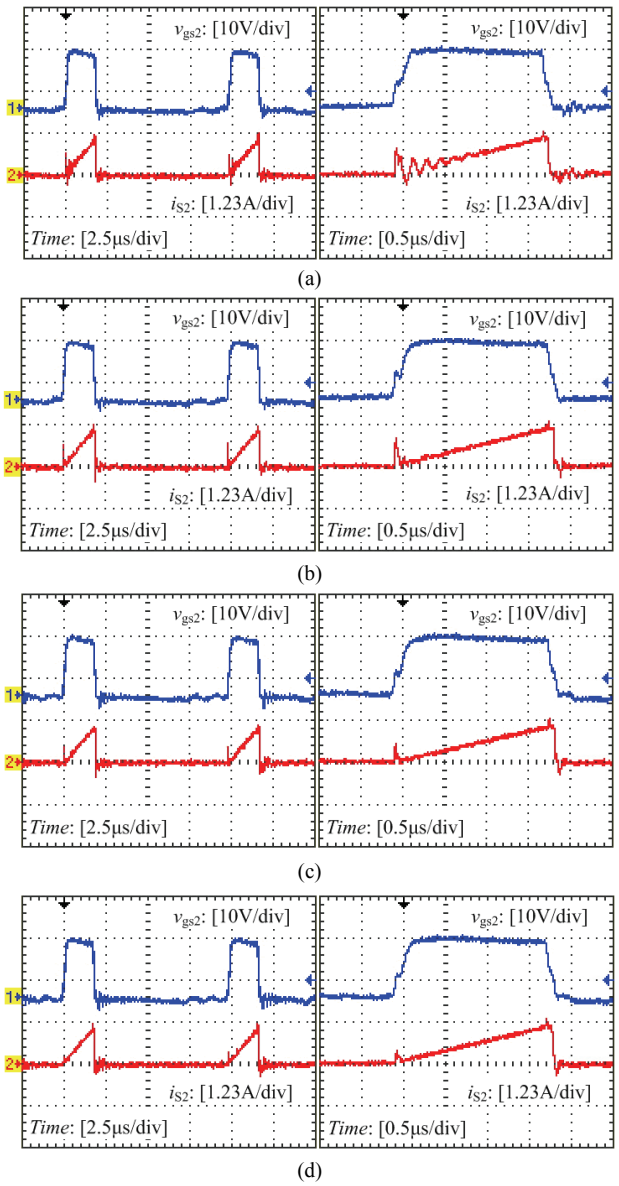

Fig. 14. Driving and current of S_2 (V_i=750V and P_o=60W). (a) T_a is adopted. (b) T_b is adopted. (c) T_c is adopted. (d) T_d is adopted.

that if turns number (N_p) is identical, the influence of the stray capacitors decreases when p increases. 4) From Figs. 12 and 13, it can be seen that the stray capacitance effects of the Z-type winding are slightly lower than those of the C-type winding.

Fig. 14 shows driving and current waveforms of S_2 when various transformers are adopted, where P_o=60W and V_i=750V. When compared to Figs. 10-13, it can be seen that when P_o increases, the stray capacitances effect becomes less serious, and the stray capacitances effect difference becomes less obvious in the prototype with various transformers.

Table IV shows conversion efficiency results of this prototype (η_a, η_b, η_c and η_d) when various transformers (T_a, T_b, T_c and T_d) are adopted, respectively. It can be seen that the efficiency of the prototype with the transformer T_c or T_d is

TABLE IV
EFFICIENCY RESULTS OF THE PROTOTYPE

V_i/V	300	450	600	750
η_a/% (P_o=16W)	81.34	81.46	82.49	81.01
η_a/% (P_o=60W)	85.60	85.67	85.37	84.51
η_b/% (P_o=16W)	81.16	81.41	81.00	80.07
η_b/% (P_o=60W)	85.02	84.21	84.07	83.40
η_c/% (P_o=16W)	82.98	83.36	82.04	81.47
η_c/% (P_o=60W)	85.56	86.46	85.84	85.46
η_d/% (P_o=16W)	83.77	84.05	83.14	81.52
η_d/% (P_o=60W)	85.94	86.56	86.06	85.83

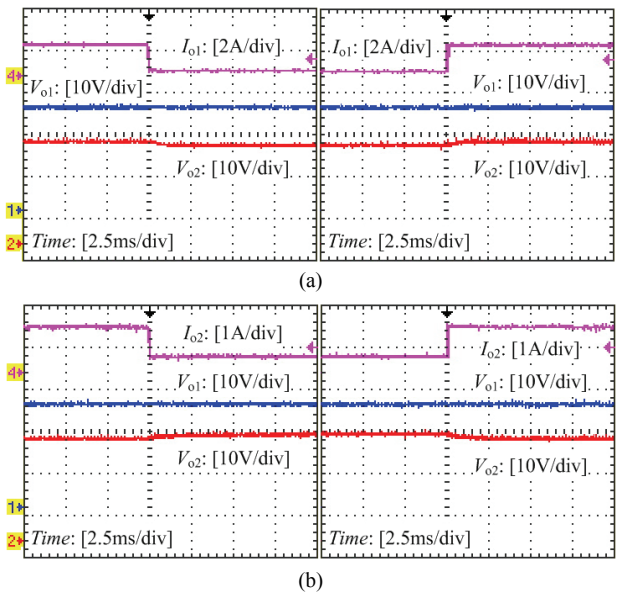

Fig. 15. Output waveforms of the prototype with T_a. (a) V_{o1} and V_{o2} to a step change of I_{o1} (I_{o2}=1A). (b) V_{o1} and V_{o2} to a step change of I_{o2} (I_{o1}=1.5A).

obviously higher than that of the prototype with the transformer T_a or T_b. It can also be seen that the efficiency difference of the prototype with each transformer increases when P_o decreases, which is due to the difference's increasing of the stray capacitances effect.

Figs. 15-18 show output voltage and current waveforms of the prototype when various transformers are adopted (the other experimental conditions are identical in these results). It can be seen that with the designed arrangement of the secondary windings, good performance of the multiple-output cross-regulation feature has been achieved in the prototype with each transformer.

From the above verification, it can be seen that when compared to the transformers T_a and T_b, the transformers T_c and T_d are more suitable for this prototype. Comparatively, T_c is slightly easier to manufacture than T_d, and the stray capacitances effect of T_d is slightly less serious than that of T_c.

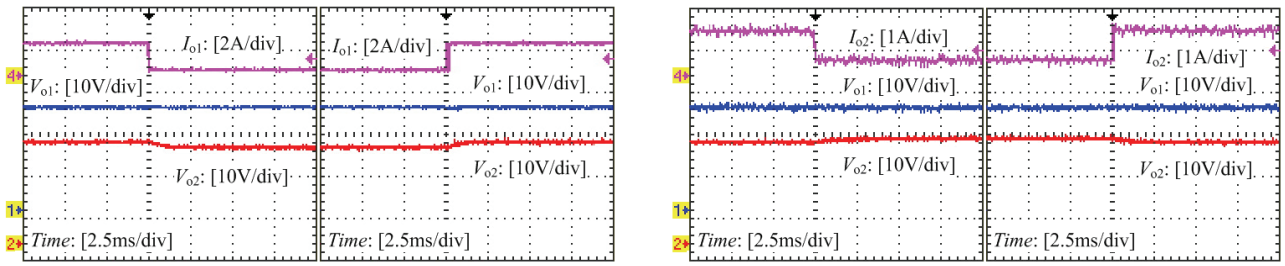

(a) (b)

Fig. 16. Output waveforms of the prototype with T_b. (a) V_{o1} and V_{o2} to a step change of I_{o1} (I_{o2}=1A). (b) V_{o1} and V_{o2} to a step change of I_{o2} (I_{o1}=1.5A).

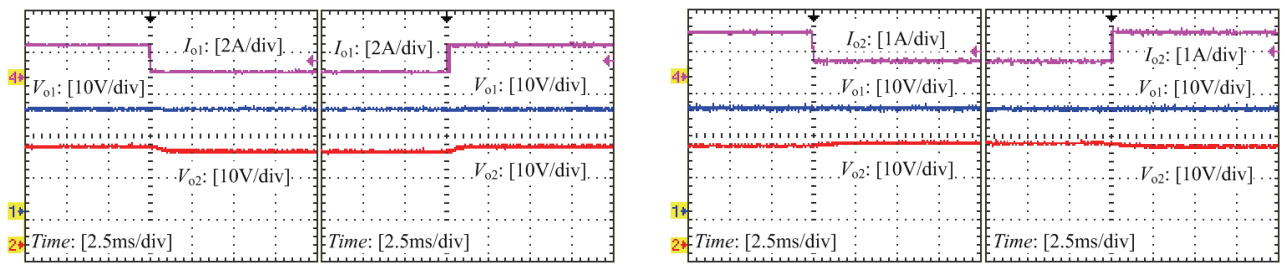

(a) (b)

Fig. 17. Output waveforms of the prototype with T_c. (a) V_{o1} and V_{o2} to a step change of I_{o1} (I_{o2}=1A). (b) V_{o1} and V_{o2} to a step change of I_{o2} (I_{o1}=1.5A).

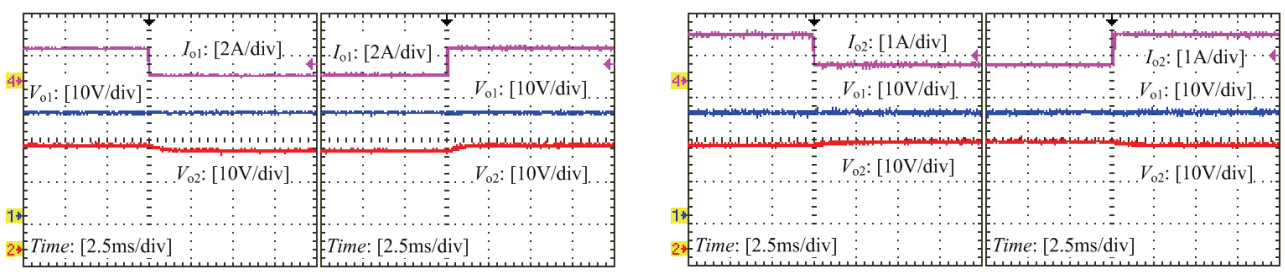

(a) (b)

Fig. 18. Output waveforms of the prototype with T_d. (a) V_{o1} and V_{o2} to a step change of I_{o1} (I_{o2}=1A). (b) V_{o1} and V_{o2} to a step change of I_{o2} (I_{o1}=1.5A).

VI. CONCLUSIONS

Aiming at high-voltage applications, transformer windings schemes of a multiple-output two-transistor flyback auxiliary power supply are analyzed and designed. The stray capacitances effect analysis shows that: 1) the stray capacitances effect is more serious in the high-voltage low-power applications, 2) the stray capacitance effect in each winding can be suppressed through the optimal design of its turns number and layer number, and 3) the stray capacitance effect of each winding can be affected by the winding structures, such as the C-type and Z-type. A coupling analysis of the secondary windings shows that the coupling coefficient of the secondary windings should be as high as possible to improve the cross-regulation feature of multiple-output circuits. Finally, based on an analysis of the stray capacitances effect between the primary and secondary windings, the windings arrangements of the transformer are analyzed and designed. In addition, they are verified by experimental results obtained from a 60W laboratory prototype.

ACKNOWLEDGMENT

This work was supporting by the National Natural Science Foundation of China (51677056), the Natural Science Foundation of Heilongjiang Province (E2016052), the Research and Development Project of Science and Technological Achievements in Provincial Universities of Heilongjiang Education Department (TSTAU-C2018014), and the Heilongjiang University Fundamental Research Funds for the Heilongjiang Province Universities (RCYJTD 201802).

REFERENCES

[1] X. Chen, W. Chen, X. Yang, Y. Han, X. Hao, and T. Xiao, "Research on a 4000-V-ultrahigh-input-switched-mode

power supply using series-connected MOSFETs," *IEEE Trans*. *Power Electron*., Vol. 33, No. 7, pp. 5995-6011, Jul. 2018.

[2] A. Gandomkar, A. Parastar, and J. Seok, "High-power multilevel step-up dc/dc converter for offshore wind energy systems," *IEEE Trans*. *Ind. Electron*., Vol. 63, No. 12, pp. 7574-7585, Dec. 2016.

[3] W. Li, Q. Jiang, Y. Mei, C. Li, Y. Deng, and X. He, "Modular multilevel dc/dc converters with phase-shift control scheme for high-voltage dc-based systems," *IEEE Trans*. *Power Electron*., Vol. 30, No. 1, pp. 99-107, Jan. 2015.

[4] W. Yang, Z. Zhang, and S. Yang, "A new control strategy for input voltage sharing in input series output independent modular dc-dc converters," *J. Power Electron.*, Vol. 17, No. 3, pp. 632-640, May 2017.

[5] L. Qu and D. Zhang, "Input voltage sharing control scheme for input series and output series dc/dc converters using paralleled MOSFETs," *IET Power Electron*., Vol. 11, No. 2, pp. 382-390, Feb. 2018.

[6] J. Liu, X. Yang, X. Hao, T. Liu, and M. Zhao, "Design of auxiliary power supply for high voltage power electronics devices," in *Proc*. *IEEE IPEMC,* pp. 1661-1665, 2012.

[7] L. Hu, C. Sun, Z. Zhao, and S. Ai, "Design of wide-range high voltage input low voltage output dc-dc auxiliary power supply," *Trans*. *China Elect*. *Soc*. Vol. 30, No. 3, pp. 103-114, Feb. 2015.

[8] F. Yan and Y. Liang, "Design and realization of a photovoltaic auxiliary power supply," *Power Electron*., Vol. 44, No. 8, pp. 14-16, Aug. 2010.

[9] P. Grbovic, "Master/slave control of input-series-and output-parallel-connected converters: concept for low-cost high-voltage auxiliary power supplies," *IEEE Trans*. *Power Electron*., Vol. 24, No. 2, pp. 316-328, Jul. 2009.

[10] S. Zong, Q. Zhu, W. Yu, and A. Huang, "Auxiliary power supply for solid state transformer with ultra high voltage capacitive driving," in *Proc*. *IEEE APEC,* pp. 1008-1013, 2015.

[11] A. Rodriguez, M. Rogina, M. Saeed, D. Lamar, M. Arias, M. Lopez, and F. Briz, "Auxiliary power supply based on a modular isop flyback configuration with very high input voltage," in *Proc*. *IEEE ECCE,* pp. 1-7, 2015.

[12] B. Hu, Z. Wei, H. Li, D. Xing, R. Na, J. Brothers, and J. Wang, "A gate drive with active voltage divider based auxiliary power supply for medium voltage SiC device in high voltage applications," in *Proc*. *IEEE APEC,* pp. 2979-2985, 2018.

[13] T. Meng, C. Li, H. Ben, and J. Zhao, "An input-series flyback auxiliary power supply scheme based on transformer-integration for high-input voltage applications," *IEEE Trans*. *Power Electron*., Vol. 31, No. 9, pp. 6383-6393, Sep. 2016.

[14] T. Meng, Y. Song, Z. Wang, H. Ben, and C. Li, "Investigation and implementation of an input-series auxiliary power supply scheme for high-input-voltage low-power applications," *IEEE Trans*. *Power Electron*., Vol. 33, No. 1, pp. 437-447, Jan. 2018.

[15] P. Thummala, H. Schneider, Z. Zhang, Z. Ouyuan, A. Knott, and M. Andersen, "Efficiency optimization by considering the high-voltage flyback transformer parasitics using an automatic winding layout technique," *IEEE Trans*. *Power Electron*., Vol. 30, No. 10, pp. 5755-5767, Oct. 2015.

[16] W. Wu, J. Zou, and Y. Chen, "Design of resonance parameters for high-voltage dc power supply considering distributed capacitance," *Elect. Power Autom. Equip.*, Vol. 29, No. 9, pp. 26-31, Sep. 2009.

[17] H. Schneider, P. Thummala, L. Huang, Z. Ouyang, A. Knott, Z. Zhang, and M. Andersen, "Investigation of transformer winding architectures for high voltage capacitor charging applications," in *Proc*. *IEEE APEC,* pp. 334-341, 2014.

[18] S. Hong, S. Ji, Y. Jung, and C. Roh, "Analysis and design of a high voltage flyback converter with resonant elements," *J. Power Electron.*, Vol. 10, No. 2, pp. 107-114, Mar. 2010.

[19] Z. Zhao, C. Gong, and H. Qin, "Effect factors on stray capacitances in high frequency transformers," *Proc. China Soc. Elect. Eng.,* Vol. 28, No. 9, pp. 55-60, Mar. 2008.

[20] J. Dong, W. Chen, and Z. Lu, "Modelling and analysis of capacitive Effects in high-frequency transformer of SMPS," *Proc. China Soc. Elect. Eng.,* Vol. 27, No. 11, pp. 121-126, Nov. 2007.

[21] P. Ranstad and H. Nee, "On the distribution of ac and dc winding capacitances in high-frequency power transformers with rectifier loads," *IEEE Trans*. *Ind. Electron*., Vol. 58, No. 5, pp. 1789-1798, May 2011.

[22] S. Wang and F. Lee, "Analysis and applications of parasitic capacitance cancellation techniques for EMI suppression," *IEEE Trans*. *Ind. Electron*., Vol. 57, No. 9, pp. 3109-3117, Sep. 2010.

[23] J. Liu, T. Guo, L. Chang, and X. He, "Effects of the parasitic capacitance on characteristics of series resonant converters," *Proc. China Soc. Elect. Eng.,* Vol. 32, No. 15, pp. 16-24, May 2012.

[24] N. Shafiei, M. Pahlevaninezhad, H. Farzanehfard, A. Bakhshai, and P. Jain, "Analysis of a fifth-order resonant converter for high-voltage dc power supplies," *IEEE Trans*. *Power Electron*., Vol. 28, No. 1, pp. 85-100, Jan. 2013.

[25] P. Musznicki, P. Chrzan, M. Rucinski, and M. Kolincio, "Adaptive estimation of the transformer stray capacitances for dc-dc converter modelling," *IET Power Electron*., Vol. 9, No. 15, pp. 2865-2870, Nov. 2016.

[26] L. Dalessandro, F. Cavalcante, and J. Kolar, "Self-capacitance of high-voltage transformers," *IEEE Trans*. *Power Electron*., Vol. 22, No. 5, pp. 2081-2092, Sep. 2007.

[27] D. Fu, S. Wang, P. Kong, F. Lee, and D. Huang, "Novel techniques to suppress the common-mode EMI noise caused by transformer parasitic capacitances in dc-dc converters," *IEEE Trans*. *Ind. Electron*., Vol. 60, No. 11, pp. 4968-4977, Nov. 2013.

[28] J. Ji, X. Zhang, W. Chen, S. An, and X. Yang, "A winding method of high frequency high voltage transformer," in *Proc*. *IEEE ECCE,* pp. 1649-1651, 2017.

[29] M. Saket, M. Ordonez, and N. Shafiei, "Planar transformers with near-zero common-mode noise for flyback and forward converters," *IEEE Trans*. *Power Electron*., Vol. 33, No. 2, pp. 1554-1571, Feb. 2018.

[30] H. Zhang, S. Wang, Y. Li, Q. Wang, and D. Fu, "Two-capacitor transformer winding capacitance models for common-mode EMI noise analysis in isolated dc-dc converters," *IEEE Trans*. *Power Electron*., Vol. 32, No. 11, pp. 8458-8469, Nov. 2017.

Xianzeng Meng was born in Henan Province, China, in 1992. He received his B.S. degree in Information and Communication Engineering from Henan Polytechnic University, Zhengzhou, China, in 2016. He is presently working towards his M.S. degree in Electrical Engineering at Heilongjiang University, Harbin, China. His current research interests include high frequency power conversion techniques and their applications.

Chunyan Li was born in Heilongjiang Province, China, in 1980. She received her B.S. degree in Automation from Heilongjiang University, Harbin, China, in 2003; and her M.S. and Ph.D. degrees in Electrical Engineering from the Harbin Institute of Technology, Harbin, China, in 2005 and 2010, respectively. Since 2014, she has been an Associate Professor in the School of Mechanical and Electrical Engineering, Heilongjiang University. Her current research interests include the design and control of permanent magnetic motors.

Tao Meng was born in Liaoning Province, China, in 1980. He received his B.S., M.S. and Ph.D. degrees in Electrical Engineering from the Harbin Institute of Technology, Harbin, China, in 2003, 2005 and 2010, respectively. Since 2018, he has been a Professor in the School of Mechanical and Electrical Engineering, Heilongjiang University, Harbin, China. His current research interests include high frequency ac/dc and dc/dc conversion techniques, power factor correction techniques, and magnetic integration techniques and their applications.

Yanhua An was born in Xinjiang Province, China, in 1994. He received his B.S. degree in Process Equipment and Control Engineering from Southwest Petroleum University, Chengdu, China, in 2016. He is presently working toward his M.S. degree in Electrical Engineering at Heilongjiang University, Harbin, China. His current research interests include high frequency power conversion techniques and their applications.